Hindawi
Journal of Electrical and Computer Engineering
Volume 2022, Article ID 7456333, 22 pages
https://doi.org/10.1155/2022/7456333

Research Article

Performance of Various Voltage Stability Indices in a Stochastic Multiobjective Optimal Power Flow Using Mayfly Algorithm

Rebeccah Kyomugisha,[1] **Christopher Maina Muriithi**,[2] **and George Nyauma Nyakoe**[3]

[1]*Electrical Engineering Department, Pan African University Institute for Basic Sciences, Technology and Innovation, Nairobi, Kenya*
[2]*Electrical Engineering Department, Murang'a University of Technology, Murang'a, Kenya*
[3]*Electrical and Computer Engineering Department, Jomo Kenyatta University of Agriculture and Technology, Nairobi, Kenya*

Correspondence should be addressed to Rebeccah Kyomugisha; beckykyomugisha@gmail.com

Received 26 February 2022; Revised 28 March 2022; Accepted 13 April 2022; Published 29 April 2022

Academic Editor: Yang Li

The performance of voltage stability indices in the multiobjective optimal power flow of modern power systems is presented in this work. Six indices: the Voltage Collapse Proximity Index (VCPI), Line Voltage Stability Index (LVSI), Line Stability Index (Lmn), Fast Voltage Stability Index (FVSI), Line Stability Factor (LQP), and Novel Line Stability Index (NLSI) were considered as case studies on a modified IEEE 30-bus consisting of thermal, wind, solar and hybrid wind-hydro generators. A multiobjective evaluation using the multiobjective mayfly algorithm (MOMA) was performed in two operational scenarios: normal and contingency conditions, using the MATLAB–MATPOWER toolbox. Fuzzy Decision-Making technique was used to determine the best compromise solutions for each Pareto front. To evaluate the computational efficiency of the case studies, a preference selection index was used. The results indicate that VCPI and NLSI yielded the best-optimized system performance in minimizing generation costs, transmission loss reduction, and simulation time for normal and contingency conditions. The best-case studies also promoted the most scheduled reactive power generation from renewable energy sources (RES). On average, the VCPI index contributed the highest penetration level from RES (13.40%), while the Lmn index had the lowest. Overall, VCPI and Lmn index provided the best and worst average performance in both operating scenarios, respectively. Also, the MOMA algorithm demonstrated superior performance against the multiobjective harris hawks algorithm (MHHO), multiobjective Jaya algorithm (MOJAYA), multiobjective particle swarm algorithm (MOPSO), and nondominated sorting genetic algorithm III (NSGA-III) algorithms. In all, the proposed approach yields the lowest system cost and loss compared to other methods.

1. Introduction

Over the recent past, increasing the load demand has brought about different power systems problems in terms of power transmission congestion and constraints. The challenges are mainly attributed to maintaining the stability of the power system at its permissible level [1, 2]. One of the inexpensive ways to ensure system stability and security is to incorporate voltage stability indices in the conventional optimal power flow (OPF) problem [3]. The traditional OPF goal includes coal-fired power plants that use fossil fuels. With the current drive to combat global warming and climate change, there is increasing global use of renewable energy sources (RES) in modern power systems [4]. Therefore, an OPF analysis that considers these nonconventional energy units is necessary [5]. The addition of voltage stability indices (VSI) in optimal flow problems has already proven to be a significant voltage stability enhancement for fossil-based power systems, especially during normal and contingency operating conditions [3, 6–8]. However, optimization and stability remain challenging with the high penetration levels of variable renewable energy

power [9, 10]. Therefore, to ensure system stability in modern power systems, the voltage stability constrained optimal power flow (VSC-OPF) must be carried out in a system integrated with renewable energy sources (RES) such as wind, solar, and hybrid RES.

Due to the fact that the OPF problem is multimodal, nonlinear, and nonconvex, classical approaches are not always appropriate and cannot guarantee a global solution. Researchers in [11] provide a comprehensive review of these approaches. The use of sensitivity analysis and gradient-based search [12] reveals that several of these techniques in [11], such as the Newton approach [13], linear programming [14], quadratic programming [15], sequential programming [16], among others, exhibit strong convergence characteristics. However, they struggle with integer and discrete variables. Furthermore, it is challenging to develop these algorithms while considering multiobjective OPF problems [17].

To address the drawbacks of the classical techniques, numerous heuristic solution methods for tackling the OPF problem have been devised. In [18], the Heap Optimization Algorithm (HOA) was used to solve the OPF of wind-solar hybrid IEEE bus systems. Firstly, the authors used HOA to optimally place RESs on buses where the lowest cost is observed for 24 hours. The authors then evaluated the OPF considering RES penetration and varying loading conditions. A MOPSO/Fuzzy Membership Function (FMF) method was used in [19] to solve the multiobjective stochastic optimal power flow of a modified IEEE 30-bus system. Three objectives: fuel cost (with and without valve-effect), power loss, and carbon emissions were considered. To deal with the intermittent nature of RESs, PDF and stochastic models are used to calculate the available power. The method yielded the least cost and emissions compared to multiobjective mayfly (MOFA), Nondominated Sorting Genetic Algorithm II (NSGA-II), and multiobjective evolutionary algorithm based on decomposition (MOEA/D), among others. However, it had the highest losses of 13.77%. Syed et al., 2021, [20] used machine learning algorithms to firstly predict wind and solar penetration levels on the Indian 124-bus system. The OPF was then solved using the Improved Wind-Driven Algorithm (IWDA) to provide the hourly and long-term power output, cost, and loss using 12 cases. The technique minimizes the complexities involved in RES integration in grids. A Modified Rao-2 Algorithm was used in [4] to optimize the control variables of the OPF problem without RES, with RES, and with RES under a contingency state. Four objectives were assessed: fuel cost, transmission loss, emission, and voltage profile improvement. The method was tested on modified IEEE 30- and IEEE 118-bus systems. The RES considered were biomass, wind, solar and hydrogenerators. The MRao-2 algorithm demonstrated dominant performance over other algorithms such as ASO, TFWO, and MPSO. In [21], a novel hybrid Mayfly algorithm-Aquila Optimizer was used to solve the OPF of a modified IEEE 30-bus system consisting of wind, solar, hydro, and thermal generators. The objectives minimized included fuel cost, power loss, VSI, and emissions. Similar studies have employed metaheuristic techniques such as evolutionary multiobjective algorithm [22], hybrid differential evolution–symbiotic organisms search (HSOS) [23], Jellyfish Search Optimization [24], multiobjective adaptive guided differential evolution (MOAGDE) algorithm [25], surrogate assisted multiobjective differential evolution method [26], Levy Interior Search Algorithm [27] to solve stochastic OPF problems. Other techniques such as the two-stage approach utilizing MOPSO algorithm, fuzzy c-means (FCM) clustering and Grey relation projection [28], and the bi-criterion evolution indicator-based evolutionary algorithm (BCE-IBEA) have also been employed to solve multiobjective problems [29]. Very few of these studies consider OPF of renewable energy integrated grid considering the system stability. Yet, the system's stability becomes increasingly challenging with the intermittency of RES.

Static voltage stability analysis remains the mainstream method for assessing proximity to collapse of power systems. This is because this type of analysis method can calculate the distance between each node's voltage and the voltage collapse point relatively accurately. Thus, it can be used to improve and optimize the power system's stability [30].

Recent works reveal three main techniques for evaluating the effectiveness of voltage stability indices in optimal power flow problems of grids integrated with RES. The most commonly used method in recent literature evaluates VSIs as independent objective functions. A case study involving the minimization of the L-index in [31] yielded the greatest voltage stability improvement on a modified IEEE 30-bus incorporating RES. The improvement was 1.231% higher than other case studies that did not include VSIs. Additionally, the objective function of the VSI study also yielded the least emissions, up to 36.780% less than other case studies. However, these advantages came at the highest generation cost. Similar studies in [32], focusing on minimizing L-index as the objective function, were tested on the RE-integrated IEEE 30-bus. It was observed that the voltage stability improved by 92.93% compared to the conventional cost-function minimization case. Also, in [33], similar improvements were observed by using the voltage stability improvement as the objective function (using L-index). The VSI case study still provided the greatest stability improvement of 2.066% compared to the base case (cost minimization). From these studies using VSI as the objective function, it is observed that the main advantages of this technique are its simplicity and simulation speed, as the focus is only on one objective function.

The second technique, commonly referred to as the weighted-sum approach, employs a multiobjective approach. In this method, several objective functions are treated as one by applying weights to each function and computing the summation of the functions. Authors in [34] employed this technique to optimally place thyristor-controlled series compensators (TCSC) on IEEE 30- and IEEE 57-buses with RES by considering the minimization of two indices: a rapid voltage stability index (RVSI) and a novel line stability index (NLSI) in the OPF problem. In [35], a case study involving the minimization of the L-index, considering a combination of traditional generators and controllable PV energy sources, was also evaluated. The

analysis indicated that the addition of the L-index provided the most significant voltage stability improvement of 1.127%, higher than cases without VSI, on the IEEE 30-bus system. It is important to note that the VSC-OPF case study also provided the greatest loss and emissions reduction of 47.491%, 31.644%, compared to the case study incorporating the emissions minimization function. Thus, VSC-OPF has significant advantages of reducing dependency on fossil-based generators by lowering the emissions on thermal generators. Although this technique provides greater improvement than the first approach, it remains a challenge to assign weights to each objective function [36].

The majority of the literature discussed involves incorporating the L-index in the VSC-OPF. Voltage stability indices have a significant impact on the generation cost and general system performance of the power system. For example, comparative studies considering various voltage stability indices in [7] revealed that the Voltage Collapse Proximity Index (VCPI) and Line voltage stability index (LVSI) provided the lowest transmission loss and emissions, respectively, across all tests systems, compared to other indices. Additionally, the L-index provided the greatest maximum loadability improvement. With these varying advantages of the different indices, it is not straightforward to select the best-performing index for the ideal operation of the power system. More studies carried out in [8] compare the effectiveness of three VSIs: LVSI index, Lmn, and the Fast Voltage Stability Index (FVSI) on IEEE 30-, IEEE 57-, and IEEE 118-bus test systems. Still, the different VSIs had varying benefits in terms of power generation cost reduction, loss minimization, and voltage stability improvement. The studies showed that the LVSI index provided better system performance for IEEE 30- and IEEE 57-buses. However, for the larger system (IEEE 118-bus), the FVSI provided the most remarkable results. Such comparative studies must continue to be assessed, especially for modern power systems, including the use of clean energy technologies. This ensures the continued secure, reliable, and cost-effective operation of power systems. However, the studies carried out employed methods that do not consider the simultaneous objectives of the power systems. That is, power system operation involves multiple parameters such as stability, cost, and loss minimization that must be considered simultaneously. Thus, a multiobjective optimization involving the use of the Pareto-optimality principle is paramount. Additionally, the challenges of the power system face a set of decision problems affiliated to different parts (e.g., scheduling, investment, and operation) where decision-makers must distinguish all alternatives from cost, revenue, or risk point of view [37]. The lack of informed decision-making can compromise the stability of systems, leading to collapse in some instances. Therefore, a selection index is required to advise on the best choice of selection of voltage stability indices in modern power systems.

From the literature assessment carried out and to the best of the authors' knowledge, no studies have compared the performance of various voltage stability indices in the multiobjective optimal power of power systems considering the stochastic nature of renewable energy technologies integration. Yet, comprehensive studies have proven that multiobjective VSC-OPF provides more significant voltage stability improvement than the two approaches used in literature in normal (28.13%) and contingency conditions (by 13.60%) [6]. More so, OPF studies considering a recently developed Mayfly algorithm are scarce; yet this algorithm has proven a dominant performance due to its global search capabilities [38].

Therefore, this paper focuses on the evaluation of six voltage stability indices: VCPI, LVSI, Lmn, FVSI, line stability factor (LQP), and the novel line stability index (NLSI) in the multiobjective OPF of a system incorporating intermittent renewable energy sources. A modified IEEE 30-bus consisting of wind, solar photovoltaic (PV), and hybrid wind- small hydro generators taken from [39] is utilized to assess the performance of the VSIs based on voltage stability improvement, generation cost minimization, transmission loss reduction, and simulation speed for each VSI. A multiobjective Mayfly algorithm (MOMA) is used to obtain the Pareto optimal solutions from all case studies. Results obtained using MOMA are validated against previous literature and four other algorithms: multiobjective harris hawks algorithm (MHHO), multiobjective Jaya algorithm (MOJAYA), multiobjective particle swarm algorithm (MOPSO), and nondominated sorting genetic algorithm III (NSGAIII).

The key contributions of this paper include the following:

(i) Evaluation of the impact of voltage stability indices in the optimal power flow of a renewable energy integrated system in normal and contingency conditions

(ii) A ranking of the performance of six voltage stability indices in a multiobjective optimal power flow, using the preference selection index (PSI).

(iii) Development and assessment of the multiobjective mayfly algorithm in the optimal power flow considering renewable energy sources

(iv) Comparison of the performance multiobjective mayfly algorithm against other algorithms in a MO-OPF in terms of generation cost and loss reduction, voltage stability improvement, and simulation speed.

(v) Impact of voltage stability constrained optimal power flow on the penetration level of renewable energy sources

The rest of the article is organized as follows: Section 2 describes the objective functions to be considered for optimization. The details of the formulations also cost functions for the RES and the general constraints for the study. Section 3 provides an overview of the stochastic modeling of the RES, while Section 4 presents the computational procedure of the MOMA algorithm. Sections 5 and 6 detail the discussion of the results obtained in the study and their validation, respectively. Lastly, Section 7 highlights general deductions from all the studies performed in this paper.

2. Problem Formulation

The multiobjective optimization problem considers three objective functions: generation cost, transmission power loss, and voltage stability index.

2.1. Generation Cost. This objective consists of minimizing the total cost of thermal generators and that of RESs, including the penalty and reserve costs.

2.1.1. Thermal Power Generator Cost. The objective focuses on minimizing the total fuel generation cost. The cost function in terms of the valve-point effect is expressed through the following equation:

$$f_{Th\_\cos t}(x) = \sum_{i=1}^{n_g}\left(a_i + b_i P_{g_i} + c_i P_{g_i}^2\right) + \left|d_i \times \sin\left(e_i \times \left(P_{gi}^{\min} - P_{gi}\right)\right)\right| \frac{\$}{h}, \tag{1}$$

where $f_{Th\_cost}(x)$ and n_g are the total fuel cost and the number of thermal generators, respectively. a_i, b_i and c_i are the i th generator cost coefficients, P_{g_i} is the i-th generator active power injection, d_i and e_i are the fuel cost coefficients modeling the valve-point effect, and $P_{gi}^{\min}$ is the minimum active power generated by the i th generating unit. The cost function's extra sinusoidal term reflects valve-point effects. Valve-point effects make the economic dispatch problem nonconvex and nondifferentiable.

2.1.2. The Cost Model of Renewable Energy Sources. RES have no need for conventional fuel to generate power. However, only operation and maintenance costs are incurred if an independent system operator owns the RES. Therefore, the ISO must pay according to the contractually agreed scheduled power [39]. Hence, there is a direct cost associated with each renewable generator, expressed in equations (2)–(4) for wind, solar PV, and hybrid wind-small hydro.

$$C_W(P_W) = g_w P_W, \tag{2}$$

where P_w represents the scheduled power and g_w, the wind power direct cost coefficient.

Equation (3) is the solar PV direct cost with scheduled power P_{PV} and cost coefficient h_{pv}:

$$C_{\mathrm{PV}}(P_{\mathrm{PV}}) = h_{pv} P_{\mathrm{PV}}. \tag{3}$$

Equation (4) presents the direct cost for scheduled power for the hybrid wind-small hydro generation plants. The maximum output of the small hydro plant is 5 MW which is dependent on the river's flow rate.

$$C_{WH}(P_{WH}) = g_{wh} P_{WH} = g_{wh} P_{WH,w} + g_{wh} P_{WH,h}, \tag{4}$$

where P_{WH} is the scheduled active power output from the hybrid plant, $P_{WH,w}$ is the output power from the wind unit and $P_{WH,h}$ from the hydro plant. g_w and g_h are the wind and hydro-unit direct coefficients, respectively.

Due to the variable nature of wind energy, the actual power produced may be less or more than the scheduled power. As such, the ISO must have reserve generating capacity to meet the demand in cases of overestimation. The Reserve cost for the wind unit is computed as in the following equation [40]:

$$\begin{aligned} C_{RW,i}\left(P_{Wsh,i} - P_{Wac,i}\right) &= k_{rw,i}\left(P_{Wsh,i} - P_{Wac,i}\right) \\ &= k_{rw,i}\int_0^{P_{Wsh,i}} \left(P_{Wsh,i} - p_{W,i}\right) f_w\left(p_{w,i}\right) \mathrm{d}p_{w,i}. \end{aligned} \tag{5}$$

Suppose the power output is underestimated (there is excess power from the RES). The ISO instead pays a penalty cost by decreasing the thermal generator power output. The wind generator penalty cost is calculated as in the following equation:

$$\begin{aligned} C_{PW,i}\left(P_{Wac,i} - P_{Wsh,i}\right) &= k_{pw,i}\left(P_{Wac,i} - P_{Wsh,i}\right) \\ &= k_{pw,i}\int_{P_{Wsh,i}}^{P_{Wr,i}} \left(p_{W,i} - P_{Wsh,i}\right) f_w\left(p_{w,i}\right) \mathrm{d}p_{w,i}, \end{aligned} \tag{6}$$

where $P_{Wsh,i}$, $P_{Wac,i}$ and $P_{Wr,i}$ denote the scheduled, available, and rated powers from wind plants, respectively. $f_w(p_{w,i})$ represents the probability density function (PDF) of wind. In the same manner, the reserve cost, penalty of solar and hybrid wind hydro generators can be estimated. Table 1 indicates the coefficients for direct, reserve, and penalty costs for the different RESs considered.

Therefore, the cumulative generation cost function of the system can be computed as follows:

$$f_1(x) = f_{Th\_\mathrm{cost}}(x) + f_{\mathrm{RES\_direct}}(x) + f_{\mathrm{RES\_penalty}}(x) + f_{\mathrm{RES\_reserve}}(x) \frac{\$}{h}. \tag{7}$$

2.2. Transmission Power Loss. The second objective minimizes the transmission power loss in MW. It is given by the following equation:

$$f_2(x) = \sum_{k=1}^{N_{\mathrm{line}}} G_k\left(V_i^2 + V_j^2 - 2V_i V_j \cos\left(\theta_i - \theta_j\right)\right), \tag{8}$$

where G_k is the kth line conductance. V_i and V_j are the voltage magnitudes for sending and receiving bus respectively, along line k. θ_i and θ_j are the sending and receiving bus voltage.

2.3. Voltage Stability Improvement. The third objective function focuses on enhancing the system voltage stability by minimizing the voltage stability index (VSI) value, as shown in equation (9). The maximum value of the VSI is considered since it represents the weakest line in the system.

$$f_3(x) = \max\left(\mathrm{VSI}_i\right). \tag{9}$$

Table 1: Cost coefficients for RES.

RES	Direct cost coefficient	Reserve cost coefficient	Penalty cost coefficient
Wind	$g_w = 1.6$	$k_{rw} = 3$	$k_{pw} = 1.5$
Solar	$g_s = 1.6$	$k_{rs} = 3$	$k_{ps} = 1.5$
Small hydro	$g_h = 1.5$	$k_{rh} = 3$	$k_{ph} = 1.5$

Table 2: Details of the VSIs in the study.

VSI	Ref.	VSI computation	Unstable condition	Stable condition
Voltage Collapse Proximity Index (VCPI)	[41]	VCPI (power) $= P_r/P_r$ (max) Where P_r (max) $= V_s^2/Z\cos\varnothing/4\cos^2((\theta - \varnothing)/2)$	VCPI > 1	VCPI ≤ 1
Line Voltage Stability Index (LVSI)	[42]	LVSI $= 4\mathrm{RP}/(V_s\cos(\theta - \delta))^2$	LVSI > 1	LVSI ≤ 1
Line Stability Index (Lmn)	[43]	$L_{mn} = 4\mathrm{XQ}_r/[V_s\sin(\theta - \delta)]^2$	$L_{mn} > 1$	$L_{mn} \leq 1$
Fast Voltage Stability Index (FVSI)	[44]	FVSI $= 4Z^2Q_r/V_s^2X$	FVSI > 1	FVSI ≤ 1
Line Stability Factor (LQP)	[45]	LQP $= 4(X/V_i^2)(X/V_i^2P_i^2 + Q_j)$	LQP > 1	LQP ≤ 1
Novel Line Stability Index (NLSI)	[46]	NLSI $= P_jR + Q_jX/0.25V^2$	NLSI > 1	NLSI ≤ 1

The VSIs considered in this study are the VCPI, LVSI, Lmn, FVSI, LQP, and NLSI, whose formulations are described in Table 2. VSI increases with power flow across a transmission line.

2.4. System Constraints. There are two types of constraints to be handled: equality and inequality constraints. Equations (10)–(16) describe the details of these constraints.

(i) Equality Constraints

These consist of load flow equations that provide the system's active and reactive power balance. They are formulated as in the following equations:

$$P_{g_i} - P_{d_i} = V_i \sum_{j=1}^{N} V_j\left(G_{ij}\cos\theta_{ij} + B_{ij}\sin\theta_{ij}\right), \quad i = 1, \ldots, N, \tag{10}$$

$$Q_{g_i} - Q_{d_i} = V_i \sum_{j=1}^{N} V_j\left(G_{ij}\sin\theta_{ij} + B_{ij}\cos\theta_{ij}\right), \quad i = 1, \ldots, N, \tag{11}$$

where P_{g_i} is the real power injection at the i th generator, Q_{g_i} is the reactive power outputs of the i th generator. P_{d_i} is the load bus active power and Q_{d_i} the load reactive power at bus i. V_i and V_j are the i th and j th bus voltage magnitude. G_{ij} denotes the conductance and B_{ij} the susceptance between buses i and j. θ_{ij} represents the buses i and j phase angle difference. N is the total number of system buses.

(ii) Inequality Constraints

The inequality constraints represent the control variable limits described in equations (12)–(17):

Generator limits:

$$P_{g_i}^{\min} \leq P_{g_i} \leq P_{g_i}^{\max}, \quad i = 1, \ldots, N_g, \tag{12}$$

$$Q_{g_i}^{\min} \leq Q_{g_i} \leq Q_{g_i}^{\max}, \quad i = 1, \ldots, N_g, \tag{13}$$

$$V_{g_i}^{\min} \leq V_{g_i} \leq V_{g_i}^{\max}, \quad i = 1, \ldots, N_g. \tag{14}$$

Transmission line limits:

$$\left|S_{L_i}\right| \leq S_{L_i}^{\max}. \tag{15}$$

Load bus voltage magnitude limits:

$$V_{d_i}^{\min} \leq V_{d_i} \leq V_{d_i}^{\max}, \quad i = 1, \ldots, N_d, \tag{16}$$

where $P_{g_i}^{\min}$ and $P_{g_i}^{\max}$ are the bus i minimum and maximum active powers (thermal/RES). $Q_{g_i}^{\min}$ and $Q_{g_i}^{\max}$ are the minimum and maximum reactive power (thermal/RES) generated at bus i. $V_{g_i}^{\min}$ and $V_{g_i}^{\max}$ are the minimum and maximum generator voltages at bus i. S_{L_i} and $S_{L_i}^{\max}$ are the apparent power flow and its maximum at branch i. $V_{d_i}^{\min}$ and $V_{d_i}^{\max}$ are the minimum and maximum load voltages at bus i. $T_i^{\min}$ and $T_i^{\max}$ are the minimum and maximum transformer tap ratios at bus i.

3. Modeling the Uncertainty of RES

This paper utilizes the uncertainty modeling of the stochastic nature of the RESs carried out in various recent literature [19, 21, 24, 47].

Wind energy production is proportionate to wind speed, and wind speed probability is best represented by the Weibull PDF [48]. Solar PV power is determined by solar irradiance, and the probability distribution of solar irradiance is represented by lognormal PDF [49]. The flow rate and effective pressure head determine the power production of a small hydro plant. From previous works, it was established that Gumbel distribution is effective in the estimation of the river flow rate [48, 50]. A summary of the wind, solar and hydro PDF parameters used in this study are presented in Table 3 [19].

Figure 1 presents the probability density functions of the RES for the parameters stated in Table 3.

4. Methodology

Figure 2 shows the methodological flow process adopted in this work for each of the two operating scenarios evaluated,

Table 3: Probability Density Function parameters for the RES stochastic models.

Wind at bus 5		Solar at bus 11		Wind + Small hydro at bus 13	
Number of turbines	25	Rated power (MW)	50	Number of turbines	15
Total rated power (MW)	75	Lognormal PDF parameters	$\mu = 6$	Rated wind power	45
Weibull PDF parameters	$\alpha = 9$ $\beta = 2$		$\sigma = 0.6$	Weibull PDF parameters	$\alpha = 10$ $\beta = 2$
				Small hydro rated power (MW)	5
				Gumbel PDF parameters	$\lambda = 15$ $\gamma = 1.2$

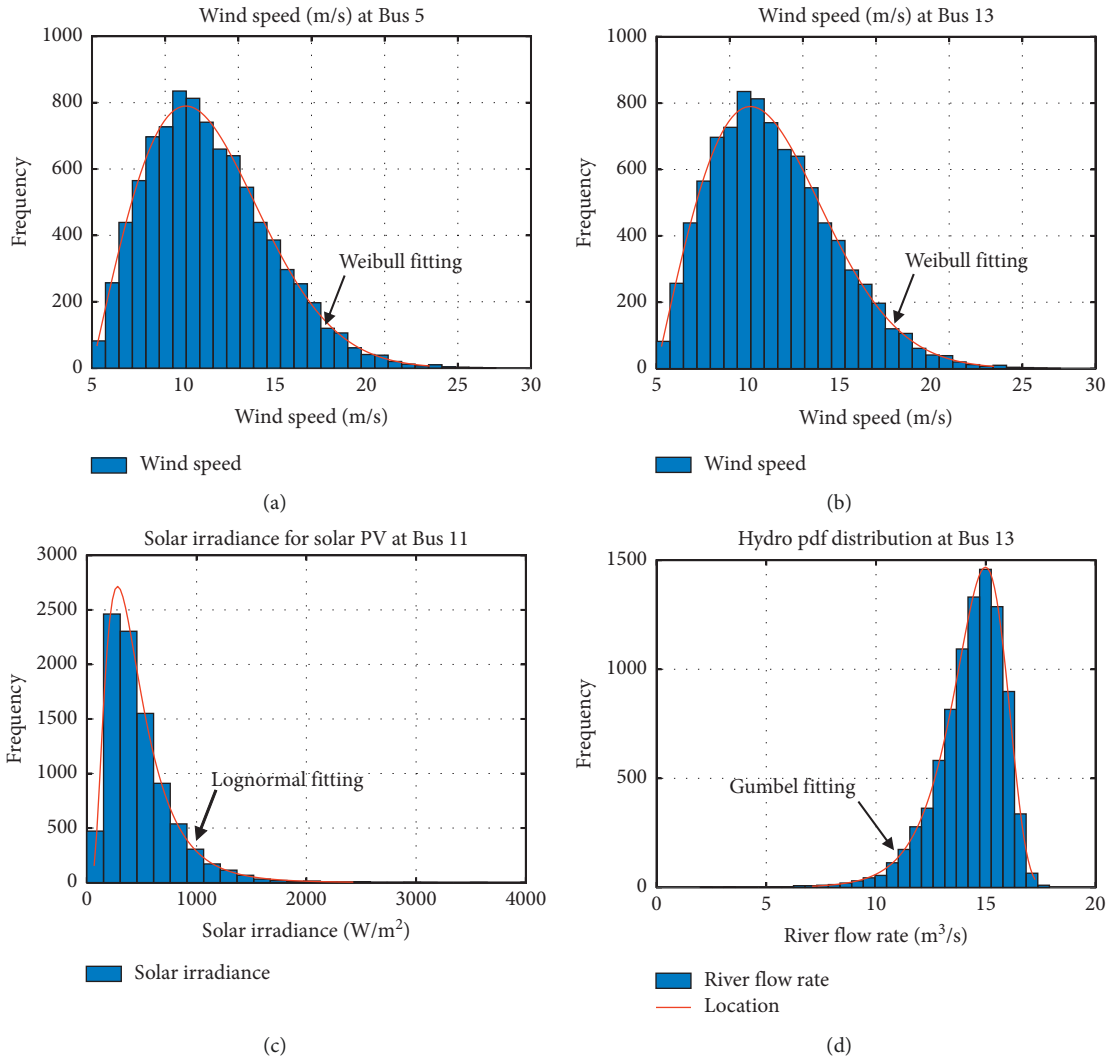

Figure 1: PDFs at (a) Bus 5 Wind, (b) Bus 13 Wind, (c) Bus 11 Solar, and (d) Bus 13 Hydro.

normal and contingency conditions. After the RES uncertainty modeling, the MOMA algorithm parameters are set to ensure convergence to local optima. Six tests were performed to achieve the best performing control parameters for the algorithm. Then, 20 independent trials were evaluated for each case study performed. Fuzzy decision-making (FDM) tool was then employed to obtain the best performing trial run in each case. Details of MOMA and the FDM are described in this section. To obtain the overall best performing VSI, a computationally efficient index, the PSI is utilized, which aggregates the best alternative from the six case studies without deciding any relative importance between attributes.

4.1. Multiobjective Mayfly Algorithm (MOMA). Zervoudakis and Tsafarakis developed Mayfly Algorithm in 2020 by mimicking the group behavior of mayflies, particularly their mating behavior [38]. Later in 2021, a multiobjective

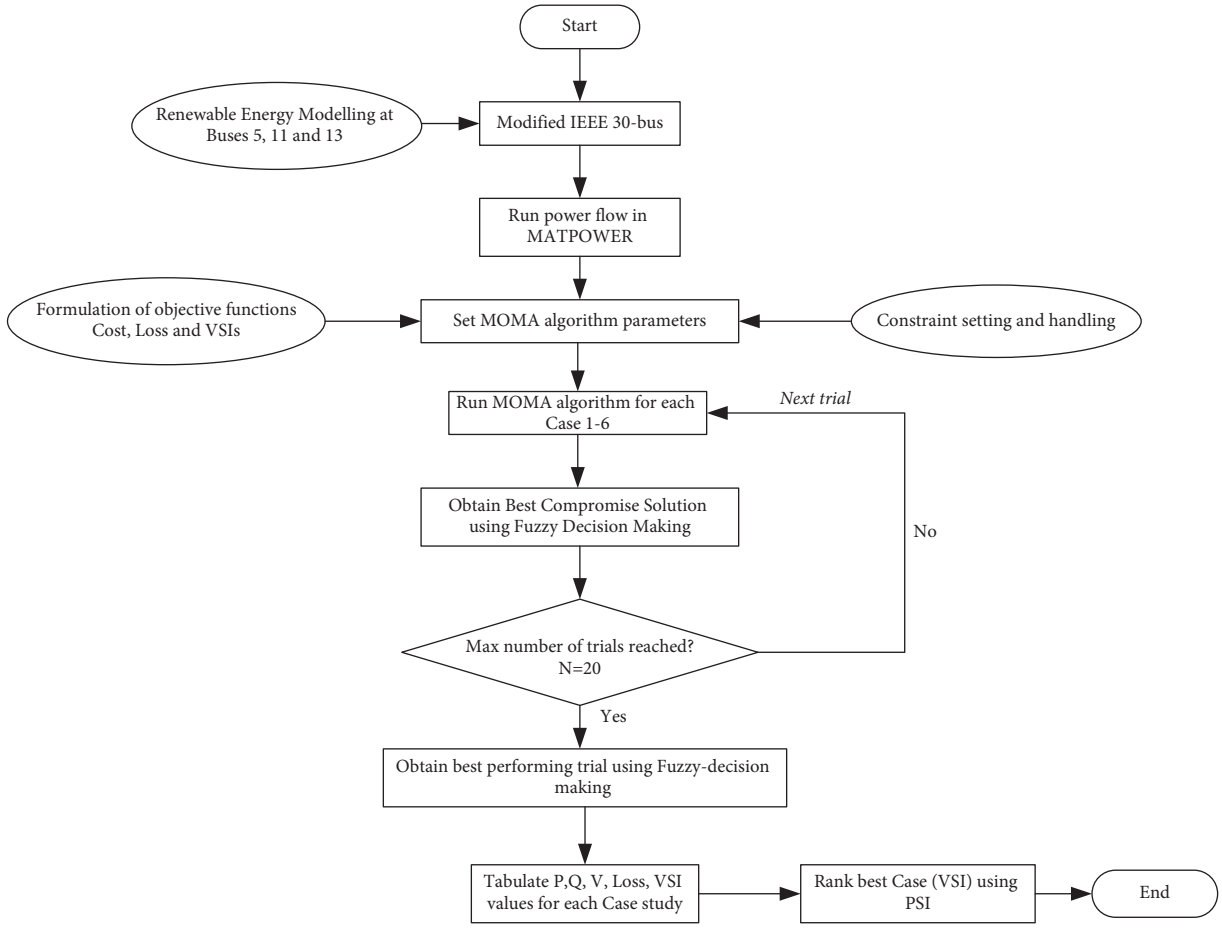

Figure 2: Methodology flow process chart.

version was developed by Liu et al. in [51]. Unlike males, female mayflies do not gather in swarms; they instead fly toward males to breed. At the start of the algorithm, the mayflies are randomly divided into two separate groups: male and female populations. The mayflies are randomly scattered in a d-dimensional space, considered candidate solutions.

Similar to the individuals in swarms of the PSO algorithm, the mayflies update the positions according to their current position $x(t)$ and velocity $v(t+1)$, as in the following equation:

$$x_{ij}^{t+1} = x_i^t + v_{ij}^{t+1}. \tag{17}$$

Since there is no single best solution in multiobjective problems, the selection of *gbest* performed by picking a random solution from the repository of nondominated solutions.

If the male mayfly is dominated by the *gbest*, (18) updates its velocity. Otherwise, the mayflies update from the current *pbest* with a random dance coefficient d.

$$v_{ij}^{t+1} = \begin{cases} v_{ij}^{t+1} = g * v_{ij}^t + a_1 e^{-\beta r_p^2}\left(pbest_{ij} - x_{ij}^t\right) + a_2 e^{-\beta r_g^2}\left(gbest_j - x_{ij}^t\right), & if\ gbest > pbest \\ g * v_{ij}^t + d * r_1, & \text{otherwise.} \end{cases} \tag{18}$$

Similarly, the movement of the female mayflies is also updated using Equation 19.

$$v_{ij}^{t+1} = \begin{cases} g * v_{ij}^t + a_2 e^{-\beta r_{mf}^2}\left(x_{ij}^t - y_{ij}^t\right), & \text{if male dominates female,} \\ g * v_{ij}^t + d * r_2, & \text{otherwise,} \end{cases} \tag{19}$$

where *pbest* and *gbest* are the local optimal and global optimal, respectively; g is the gravity coefficient; a_1, a_2, are constants to balance the values; β is the fixed visibility coefficient; r_p and r_g are Cartesian distances from the $i-th$ mayfly to the optimal local solution and the optimal global solution, respectively; r_1 and r_2 is the random number in uniform distribution and selected from the domain [−1, 1].

Figure 3 summarizes the flow chart of the multiobjective MayFly algorithm. The rest of the steps of the MOMA algorithm are detailed in [38, 51]

4.2. Fuzzy Decision-Making Technique. To find out the best compromise solution among the nondominated solutions from the Pareto front is vital in the decision-making process. Fuzzy set theory has been widely utilized to effectively select a candidate Pareto-optimal solution from among the numerous alternative solutions on the Pareto front [6]. Due to the inherent irrationality nature of the decision-makers, the $i-$ th objective function of a solution in the Pareto-optimal set, F_i, is represented by a membership function μ_i defined as follows [52]:

$$\mu_i = \begin{cases} 1, & F_i \le F_i^{\min}, \\ \dfrac{F_i^{\max} - F_i}{F_i^{\max} - F_i^{\min}}, & F_i^{\min} \le F_i \le F_i^{\max}, \\ 0, & F_i \ge F_i^{\max}, \end{cases} \tag{20}$$

where $F_i^{\max}$ and $F_i^{\min}$ are maximum and minimum values of the $i-$ th objective function, respectively. The membership function values designate the achievement level of the objective functions of a problem, and these values are between 0 and 1. For each nondominated solution k, the normalized membership function μ^k is calculated as follows:

$$\mu^k = \frac{\sum_{i=1}^{N_{obj}} \mu_i^k}{\sum_{j=1}^{M} \sum_{i=1}^{N_{obj}} \mu_i^j}. \tag{21}$$

The number of nondominated solutions is M. The best compromise solution is the one having the highest value of μ^k.

5. Results and Discussion

To assess the performance of the voltage stability indices in a multiobjective OPF problem, a MOMA algorithm was executed on a modified IEEE 30-bus consisting of wind, solar PV, and small hydro sources. It was already established in [6] that three a three-objective VSC-OPF provided better system performance than the two ones. Therefore, each VSI is formulated as part of the triobjective function alongside generation cost and loss minimization objectives in this work. The tests were considered in two operating conditions, normal and contingency. The Best Compromise Solution was obtained using the Fuzzy decision-making theory [53], whereas to obtain a ranking of the case studies, a Preference Selection Index (PSI) was employed [6, 54]. The overall computational effectiveness of the VSIs is tested in terms of cost and transmission loss reduction, voltage stability improvement, simulation time, and support for RES penetration level.

5.1. Modified IEEE 30-Bus. The modified IEEE 30-bus presented in Figure 4 and Table 4 was obtained from [39, 55]. The system comprises thirty buses, six generators, forty-one branches, and four transformers. Buses 1, 2, 5, 8, 11, and 13, indicate the locations of the generators. The active and reactive power loads are 283.4 MW and 126.2 MVAR, respectively.

5.2. Case Studies. For all analyses, the MATLAB MATPOWER toolbox was employed on an Intel (R) Core (TM) i7-2640M CPU @2.8 GHz and (RAM) 8 GB computer. Six case studies were assessed to investigate the network's performance under different conditions, as shown in Table 5. The goal is to assess the network's performance when different voltage stability indices are incorporated into the multiobjective function. The best performing VSI in each operating scenario is selected based on the Preference Selection index (PSI), whose formulations of PSI are detailed in [54]. The Best Compromise Solutions (BCS) generated from multiobjective studies using the Fuzzy Decision-Making technique are utilized to further evaluate the system performance.

5.3. Multiobjective Optimization. This section presents the results of the triobjective optimization using the multiobjective Mayfly algorithm in two operating conditions.

5.3.1. MOMA Convergence Characteristics. Heuristic techniques are sensitive to the proper selection of the control parameters. These parameters are selected through experiment. With the chosen parameters, an investigation was done to optimize the population sizes for the system. A total of 20 independent trials were carried out for each of the test runs. The population size in the present work is fixed at 20 particles in order to keep the computational requirements low. From Table 6, it is clear that a population of 20 particles in 50 iterations provides satisfactory convergence characteristics. The selection of best parameters was established using fuzzy decision making, considering the contradicting objectives of cost, loss, and voltage stability. Table 6 shows that test run four (in bold) control parameters achieve the best compromise cost, loss, and voltage stability index for Case 1.

To verify the convergence characteristics of the MOMA with the selected parameters, OPF simulation was carried out with the optimum number of particles for each system for 50 iterations; the repository population variation vs. iterations is shown in Figure 5. It can be seen that MOMA converges well in less than 50 iterations.

To ensure consistency, the MOMA algorithm is run in 20 independent trials for each of the case studies of the multiobjective OPF. The best compromise solutions obtained in each test run trial undergo another best-case selection using the fuzzy decision technique. Figure 6 shows the selection of the best compromise solution for case 1 in normal operating conditions. Details of the selected solution are provided in Table 7.

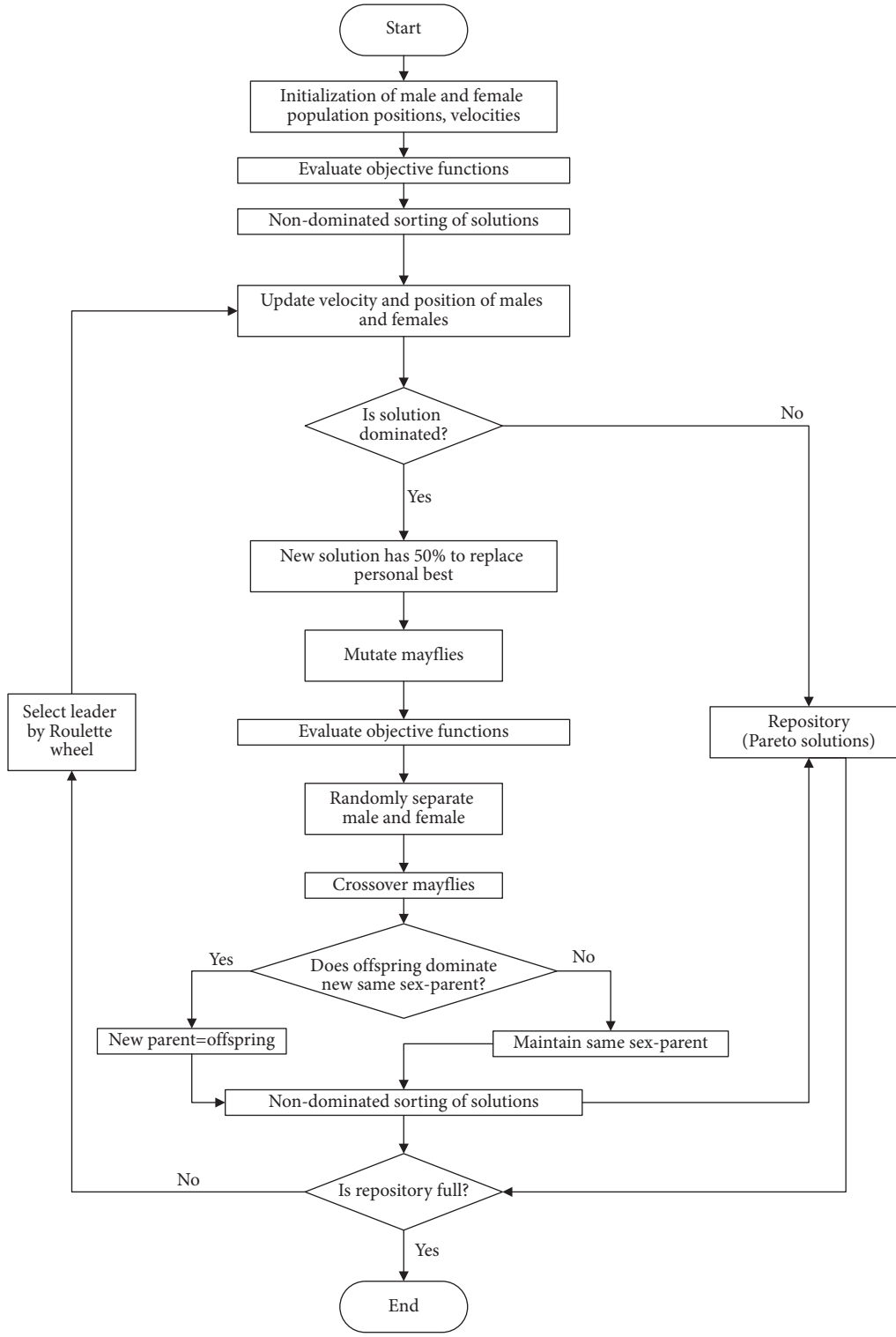

Figure 3: Flow chart of multiobjective mayfly algorithm (MOMA).

5.3.2. Normal Operating Conditions (SC-1). With the system under normal operating conditions, the results of the multiobjective optimization and their corresponding BCS (marked in red star) are presented in Figure 7.

Results in Table 7 indicate that the lowest costs were obtained in Case 3 by the Lmn index, followed by the NLSI index in Case 6. However, the case studies with the lowest costs also encounter the highest loss, as evidenced by the highest loss of 4.26 MW with Lmn index.

The lowest costs (809.68 $/h), losses (2.55 MW), and simulation time (43.132 s) are realized in Case 3 (Lmn), Case 1 (VCPI), and Case 4 (FVSI), respectively. However, it is noteworthy that the Lmn index with the lowest costs also encounters the highest losses of 4.26 MW, 66.85% more

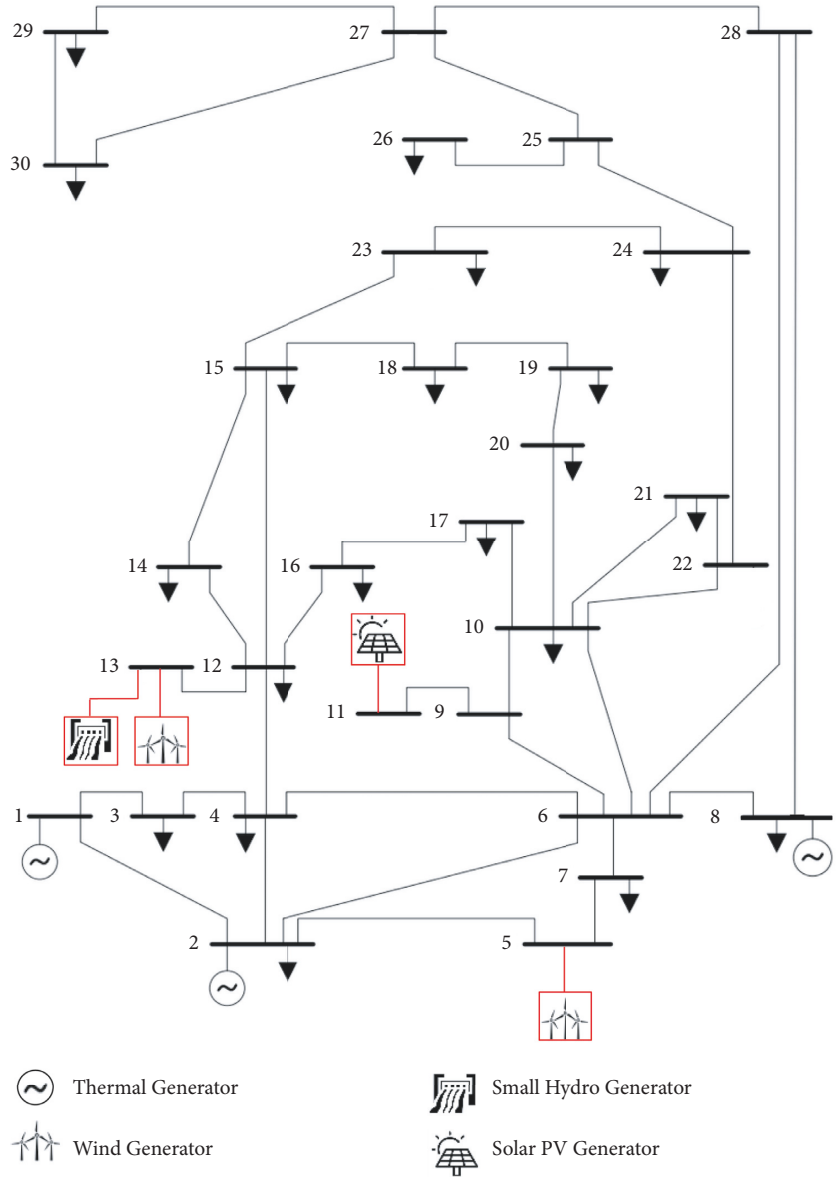

Figure 4: Modified IEEE 30-bus consisting of wind, solar, hydro, and thermal generators.

Table 4: Details of the modified IEEE 30-bus.

Bus	Type	P_{min}	Pmax	Generator cost coefficients				
				a	b	c	d	e
1	Thermal	50	140	0.00375	2	0	18	0.037
2	Thermal	20	80	0.01750	1.75	0	16	0.038
5	Wind generator	0	75	—	—	—	—	—
8	Thermal	10	35	0.00834	3.25	0	12	0.045
11	Solar PV	0	60	—	—	—	—	—
13	Wind generator + small hydro unit	0	50	—	—	—	—	—

than that of Case 1. Conversely, the VCPI index with the lowest losses also produces the highest costs. This is due to the fact that for losses to reduce, the system must generate more reactive or have the least consumption. Table 3 shows that the VCPI index (Case1) has the lowest net consumption of reactive power (Qgen), hence the lowest losses (see Figure 8).

The overall PSI ranking shows that VCPI is the most computationally efficient index, ranking highest with a PSI of 0.9562 in normal operating conditions for optimized system performance in terms of minimizing generation cost, loss, simulation time, and voltage stability improvement.

Table 5: Case studies and scenarios considered for the study.

Scenarios (SC)	Details	Objective Functions	Case 1 VCPI	Case 2 LVSI	Case 3 Lmn	Case 4 FVSI	Case 5 LQP	Case 6 NLSI
Normal operating conditions (**SC-1**)	Baseload conditions	Generation Cost ($/h) Power Loss (MW) VSI	☑	☑	☑	☑	☑	☑
Line outage contingency conditions (**SC-2**)	Line 1-2 disconnected (it has the highest VSI, therefore weakest line)	Generation Cost ($/h) Power Loss (MW) VSI	☑	☑	☑	☑	☑	☑

Table 6: Parameter setting for MOMA.

Test	MaxIt	Pop No.	Pop No. (males & females)	Repository Size	Cost ($/h)	Loss (MW)	VSI
1	20	20	20	50	858.9744	3.1975	0.3406
2	20	20	20	80	857.7473	3.5238	0.3336
3	20	20	20	20	850.8305	3.7796	0.3958
4	**50**	**20**	**20**	**20**	**862.4796**	**2.9661**	**0.3285**
5	100	20	20	20	856.511	3.3431	0.3517
6	20	20	20	20	852.5979	3.3668	0.3635

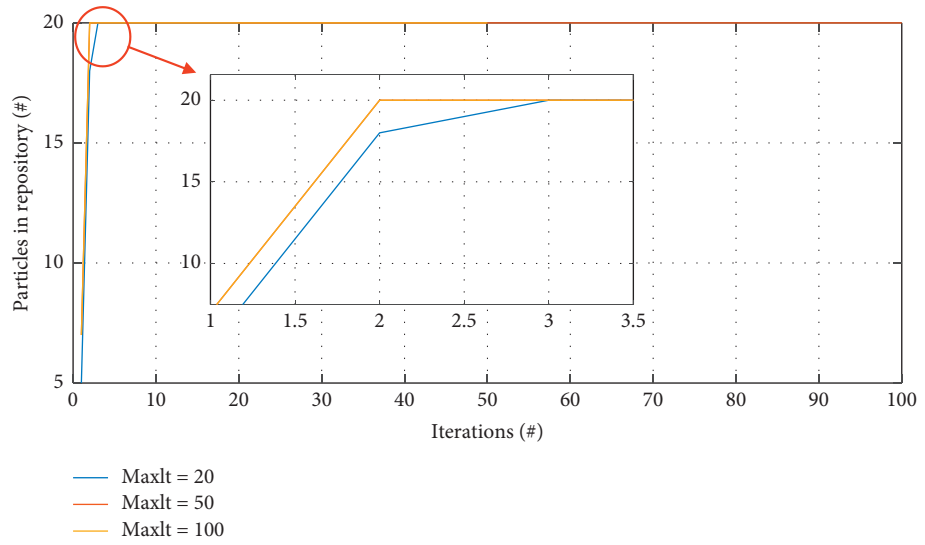

Figure 5: Convergence characteristics at different iterations.

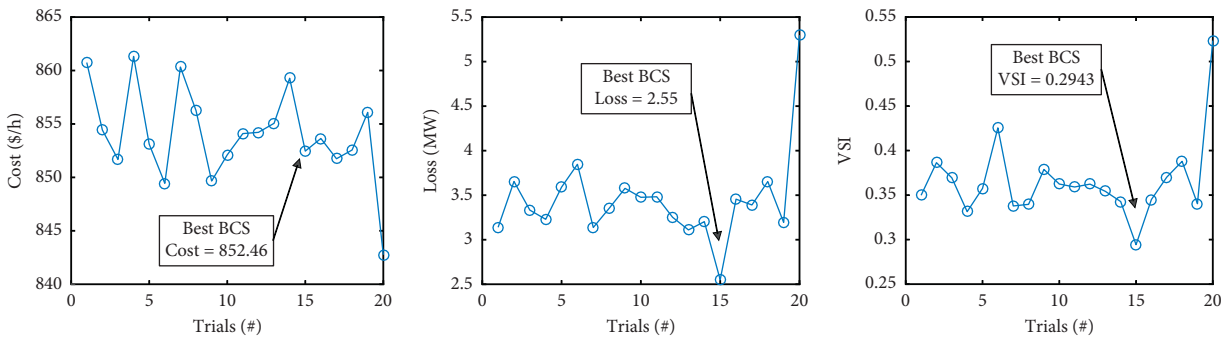

Figure 6: 20 independent trials run for case 1 SC-1.

Table 7: Best compromise solutions from the different case studies in SC-1.

Bus	Control variables	Base		Case 1	Case 2	Case 3	Case 4	Case 5	Case 6
		Min	Max	VCPI	LVSI	Lmn	FVSI	LQP	NLSI
1	P_{TH} (MW)	50	140	90.39	91.29	100.52	64.93	114.44	91.73
2	P_{TH} (MW)	20	80	51.04	57.24	50.56	38.16	56.30	58.36
5	P_{W} (MW)	0	75	70.32	62.28	47.57	58.48	58.95	68.57
8	P_{TH} (MW)	10	35	22.31	15.10	18.77	25.86	22.93	18.87
11	P_{PV} (MW)	0	60	42.50	44.80	41.50	54.89	54.26	40.68
13	P_{W+H} (MW)	0	50	42.73	38.91	34.33	35.99	36.43	40.23
	Pgen (MW)	80	440	319.29	309.62	293.24	278.31	343.30	318.44
1	Q_{TH} (MVAR)	−20	150	21.33	116.22	59.37	117.82	−0.38	21.34
2	Q_{TH} (MVAR)	−20	60	−12.45	23.58	22.61	41.70	41.55	27.37
5	Q_{W} (MVAR)	−30	35	6.46	−12.00	−5.97	20.60	−8.06	−7.29
8	Q_{TH} (MVAR)	−15	40	20.81	0.75	14.78	30.21	12.32	−1.68
11	Q_{PV} (MVAR)	−20	25	−1.29	0.14	−1.51	10.19	18.54	8.56
13	Q_{W+H} (MVAR)	−25	30	−2.88	1.37	−3.70	−9.44	−9.00	8.19
	Qgen (MVAR)	−130	340	31.97	130.05	85.58	211.08	54.96	56.49
1	V_{TH} (p.u)	0.95	1.1	1.1	1.0855	0.9672	1.058	1.1	0.95
2	V_{W} (p.u)	0.95	1.1	0.95	1.1	1.0804	1.0748	1.1	1.1
5	V_{TH} (p.u)	0.95	1.1	1.1	1.0921	1.0566	1.0755	1.1	1.1
8	V_{PV} (p.u)	0.95	1.1	1.1	1.1	1.0578	1.0755	1.1	1.1
11	V_{W+H} (p.u)	0.95	1.1	0.95	0.9873	1.0012	0.9903	0.95	0.95
13	V_{TH} (p.u)	0.95	1.1	1.1	1.086	1.0971	1.0988	1.1	1.1
	Cost ($/h)	—	—	852.46	839.66	809.68	838.27	846.88	838.72
	Loss (MW)	—	—	2.55	3.03	4.26	2.86	2.61	2.93
	VSI	—	—	0.2943	0.0843	0.1198	0.1359	0.3069	0.2023
	Simulation Time (s)	—	—	45.704	48.725	47.237	43.132	44.951	47.899
	PSI	—	—	0.9562	0.8470	0.7903	0.8316	0.8952	0.8547
	PSI ranking	—	—	1	4	6	5	2	3

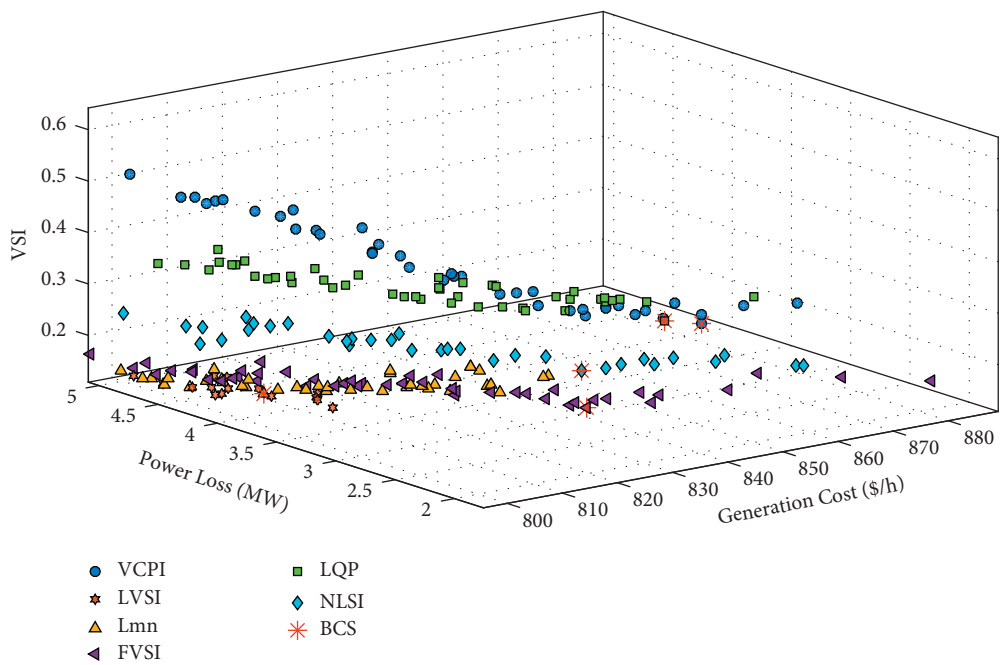

Figure 7: SC-1 Pareto-optimal solutions for the six case studies.

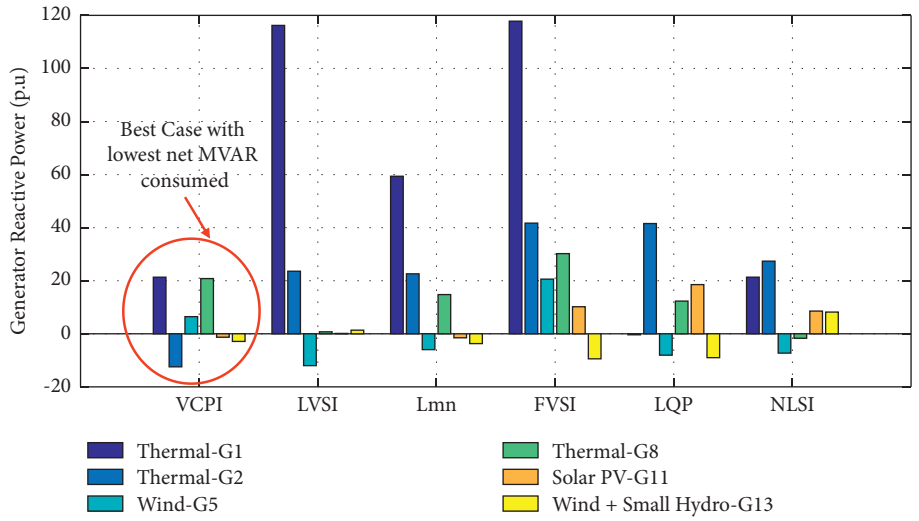

Figure 8: SC-1 Reactive power generation from the different generators.

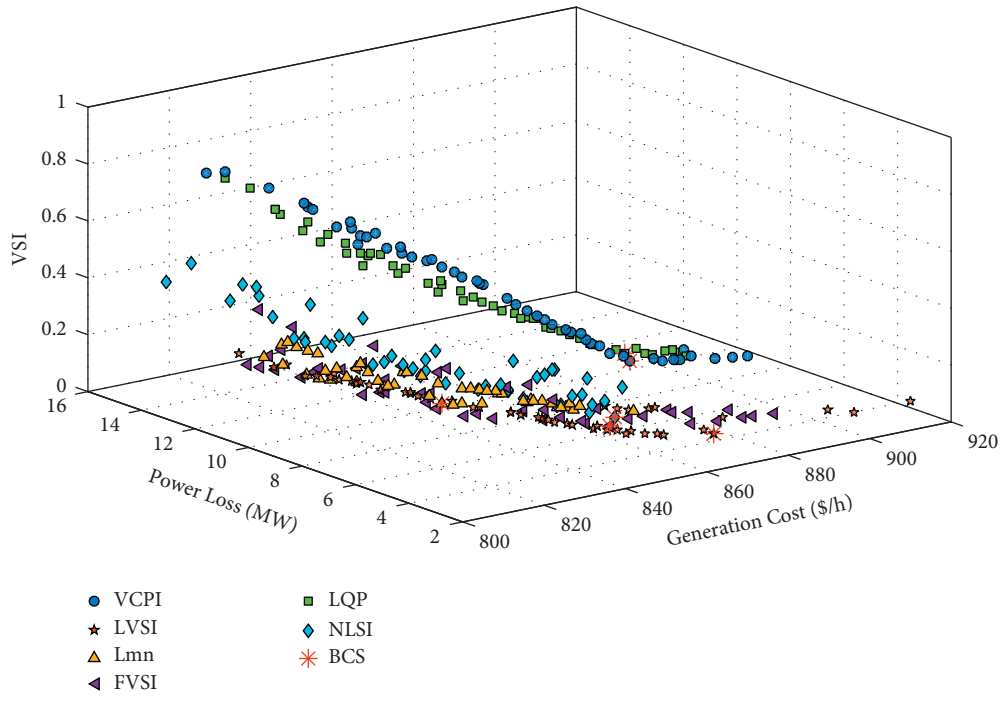

Figure 9: SC-2 Pareto-optimal solutions for the six case studies.

5.3.3. Contingency Conditions (SC-2). This study assesses voltage stability indices' impact when line 1-2 is out of service. Contingency conditions are known to change the power flows in the system, thus resulting in increased loading of lines in some instances, leading to increased losses and costs. Figure 9 shows the Pareto optimal solutions obtained from the different voltage stability indices.

From the graph in Figure 9, it can be observed that VCPI and LQP indices have the highest generation costs. However, the Pgen, Qgen, and lowest losses are realized with VCPI, NLSI, and LVSI, respectively, as seen in Table 8. The FVSI index is still the index with the shortest simulation time, whereas the greatest voltage stability improvement of 89.9% is seen with the LQP index (compared to the base SC-2 LQP index of 3.7567).

Since different indices have varying advantages in reducing generation cost, loss and simulation time, and voltage stability improvement, the PSI index helps aggregate and rank the efficiency and performance of all case studies. Therefore, in contingency conditions, the index with the best-optimized system performance is the NSLI index with a PSI value of 0.9290. Figure 10 affirms that the best performing index, NLSI, generates the most reactive power from renewable energy sources.

Table 8: Best compromise solutions from the different case studies in SC-2.

Bus	Control variables	Base		Case 1	Case 2	Case 3	Case 4	Case 5	Case 6
		Min	Max	VCPI	LVSI	Lmn	FVSI	LQP	NLSI
1	P_{TH} (MW)	50	140	61.08	113.14	119.10	84.49	88.54	100.36
2	P_{TH} (MW)	20	80	60.23	66.33	55.58	51.87	65.51	44.92
5	P_W (MW)	0	75	56.44	63.62	42.66	56.21	62.40	68.43
8	P_{TH} (MW)	10	35	22.59	27.35	17.17	27.90	18.48	22.02
11	P_{PV} (MW)	0	60	51.88	43.77	47.54	50.01	41.93	49.79
13	P_{W+H} (MW)	0	50	41.74	39.88	29.43	40.13	38.44	36.96
	Pgen (MW)	80	440	293.94	354.08	311.48	310.60	315.30	322.48
1	Q_{TH} (MVAR)	−20	150	62.34	74.86	73.92	42.82	59.94	27.18
2	Q_{TH} (MVAR)	−20	60	45.15	22.16	4.84	25.69	36.87	33.66
5	Q_W (MVAR)	−30	35	8.39	−9.79	9.87	14.75	−18.11	−10.18
8	Q_{TH} (MVAR)	−15	40	4.23	10.29	3.65	15.54	3.29	6.86
11	Q_{PV} (MVAR)	−20	25	−5.45	0.35	−3.86	12.64	10.63	−3.86
13	Q_{W+H} (MVAR)	−25	30	9.16	7.84	−6.24	−6.97	1.13	−18.54
	Qgen (MVAR)	−130	340	123.82	105.71	82.19	104.47	93.76	35.12
1	V_{TH} (p.u)	0.95	1.1	1.1	1.1	1.0997	1.0997	1.0971	1.1
2	V_W (p.u)	0.95	1.1	1.1	1.1	1.0734	1.0625	1.0984	1.0865
5	V_{TH} (p.u)	0.95	1.1	1.1	1.1	1.0592	1.0659	1.0756	1.0697
8	V_{PV} (p.u)	0.95	1.1	1.1	1.1	1.0452	1.062	1.1	1.0643
11	V_{W+H} (p.u)	0.95	1.1	0.95	0.95	1.0389	0.955	0.9628	1.0923
13	V_{TH} (p.u)	0.95	1.1	1.1	1.1	1.0827	1.0975	1.0969	1.0979
	Cost ($/h)	—	—	851.13	867.80	832.23	848.86	852.22	850.05
	Loss (MW)	—	—	3.54	2.92	7.68	3.93	3.89	3.92
	VSI	—	—	0.3641	0.0832	0.1355	0.1300	0.3767	0.1528
	Simulation Time (s)	—	—	43.607	43.41	41.739	40.867	45.264	42.958
	PSI	—	—	0.8600	0.8633	0.8185	0.8653	0.8552	0.9290
	PSI ranking	—	—	4	3	6	2	5	1

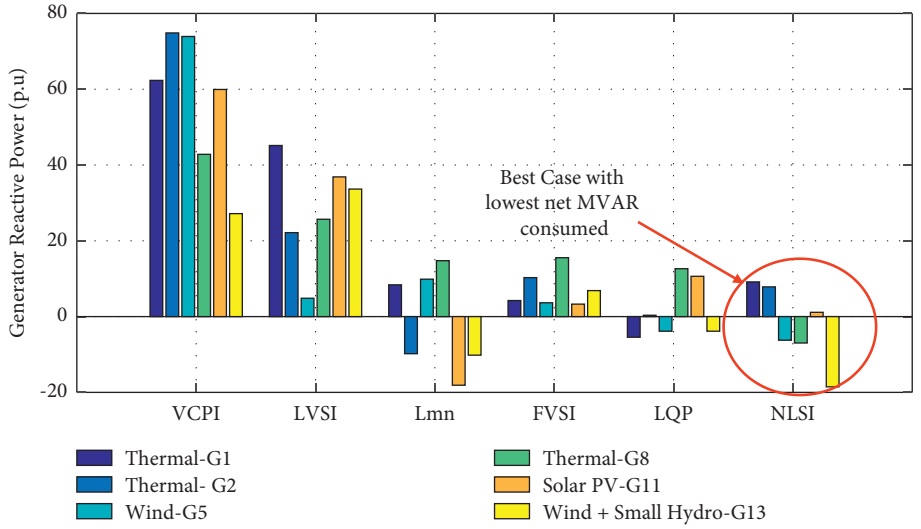

Figure 10: SC-2 Reactive power generation from the different generators.

5.4. Impact on Voltage Stability

5.4.1. Bus Voltage Magnitudes. Figures 11 and 12 indicate the bus voltage magnitude performance resulting from the different case studies. FVSI and LQP indices achieve the highest average voltage profile improvement of 0.36% compared to the base case in normal operating conditions. On the other hand, the system voltage profile improves the most in the VCPI case study (by 1.42%) during line outage conditions.

5.4.2. PV Curves. The best compromise solution obtained from the Pareto curves was used further to assess the maximum loadability of the different case studies.

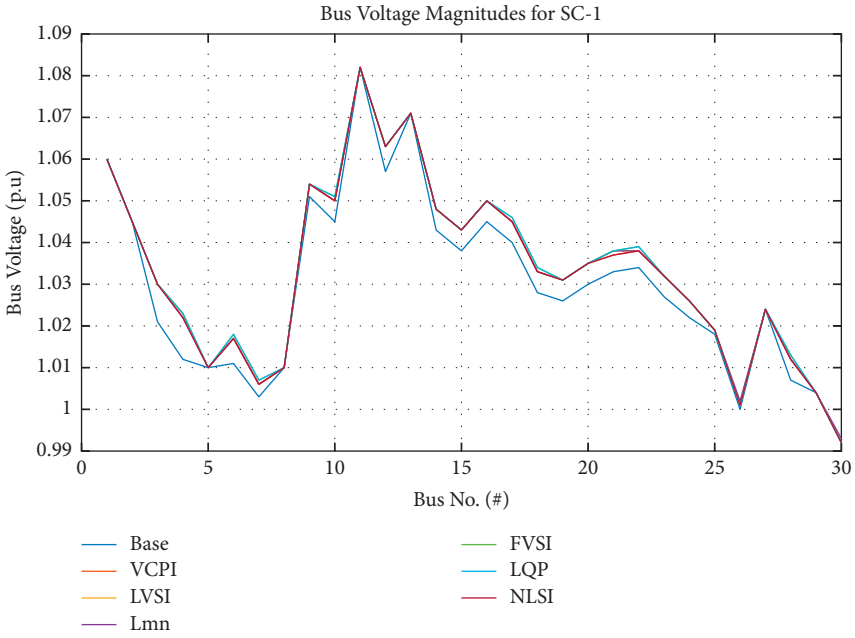

Figure 11: SC-1 bus voltage magnitudes for the different case studies.

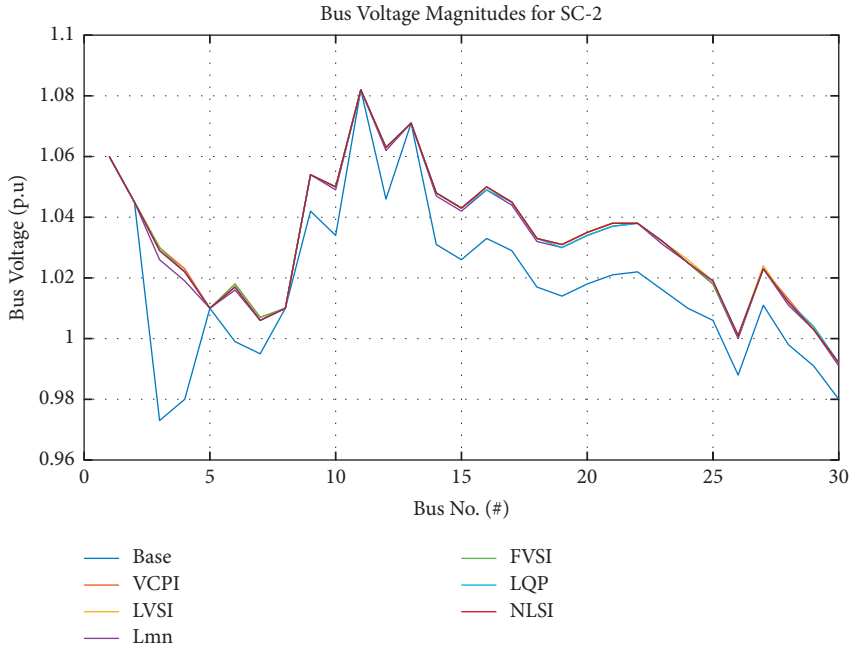

Figure 12: SC-2 bus voltage magnitudes for the different case studies.

In normal operating conditions, it is observed from Figure 13 that Case 6 (NLSI) gives the most significant load margin improvement of 10.17%. The rest of the indices improve the maximum loadability by 9.96%, 9.58%, 9.76%, 9.02%, 8.91% in Case 1, Case 2, Case 3, Case 4, and Case 5, respectively. The lowest loadability margin in SC-1 is realized with the FVSI index.

In contingency conditions, the maximum loadability of the system is improved by over 700% in all cases, as presented in Figure 14. The greatest improvement was achieved with the LVSI index and the lowest with the Lmn index.

5.5. Contribution of Renewable Energy Sources. Optimization of generation scheduling alters the system control variables, leading to varying generation power contributions from the renewables. High penetration of

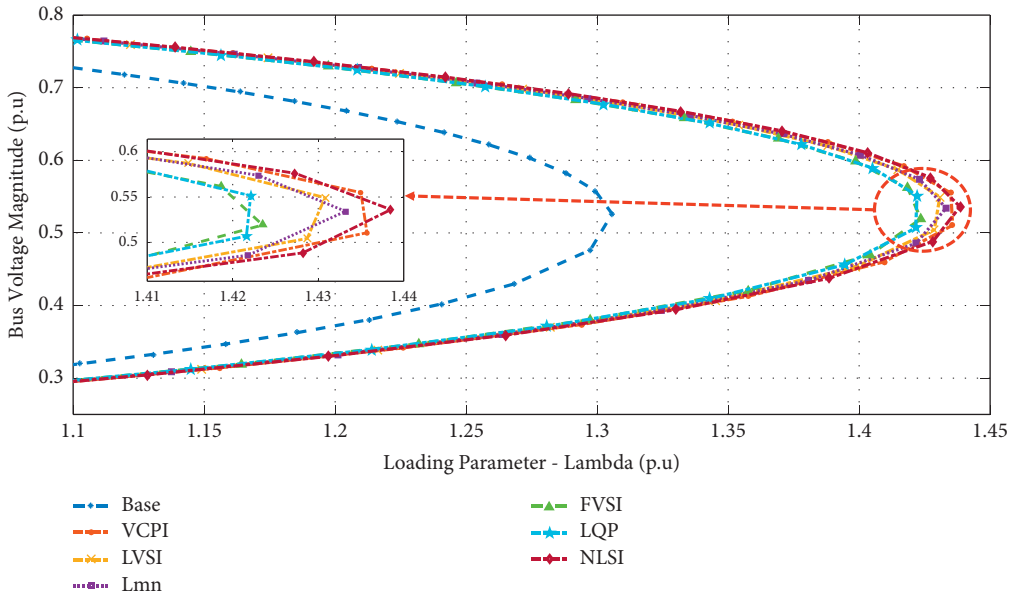

Figure 13: Maximum loadability in SC-1 by PV curves at Bus 30.

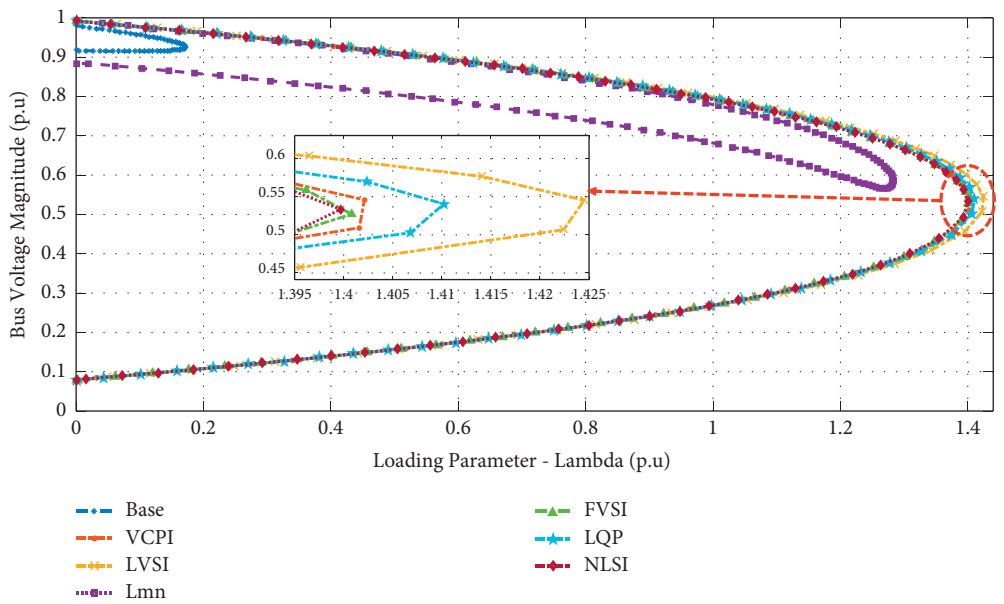

Figure 14: Maximum loadability in SC-1 by PV curves at Bus 30.

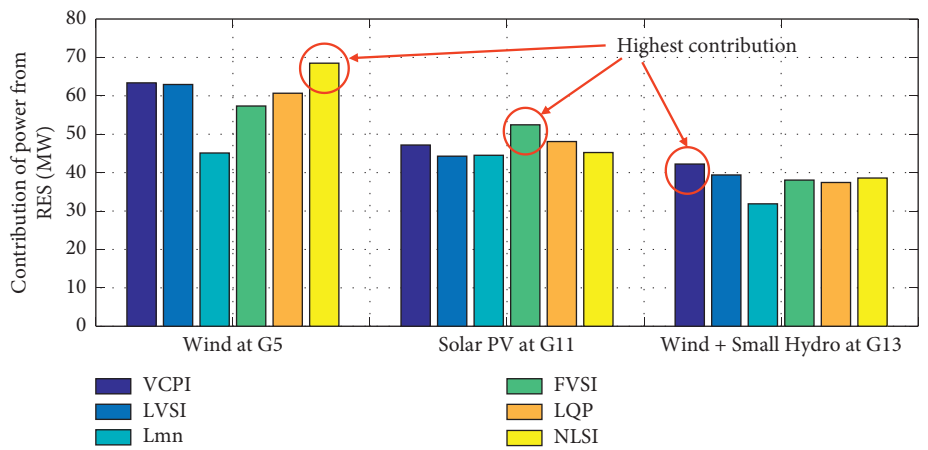

Figure 15: Contribution of power from the RES.

Table 9: Scheduled Power level of RES.

VSI	Wind			PV			Wind and Hydro			Average Overall	
	Contribution (MW)	Scheduled Power (%)	Penetration (%)	Contribution (MW)	Scheduled Power (%)	Penetration (%)	Contribution (MW)	Scheduled Power (%)	Penetration (%)	Contribution (MW)	Penetration (%)
VCPI	63.38	84.51	20.67	47.19	78.7	15.39	42.235	84.5	13.77	82.54	16.61
LVSI	62.95	83.93	18.97	44.285	73.8	13.34	39.395	78.8	11.87	78.84	14.73
Lmn	45.115	60.15	14.92	44.52	74.2	14.72	31.88	63.8	10.54	66.04	13.40
FVSI	57.345	76.46	19.47	52.45	87.4	17.81	38.06	76.1	12.93	80.00	16.74
LQP	60.675	80.90	18.43	48.095	80.2	14.61	37.435	74.9	11.37	78.64	14.80
NLSI	68.5	91.33	21.38	45.235	75.4	14.12	38.595	77.2	12.04	81.31	15.84

Table 10: Validation of SC-1 Case 1 MOMA results against other algorithms.

Algorithm	Algorithm Parameters			Best compromise Solutions			Simulation Time (s)
	Population	Iterations	Pareto Solutions at Max. Iteration	Cost ($/h)	Loss (MW)	VSI	
MOMA	20	50	20	852.464	2.554	0.294	45.704
MHHO	50	50	50	849.907	2.350	0.327	122.035
MOJAYA	50	50	25	844.826	2.719	0.3235	67.395
MOPSO	50	50	50	863.554	2.189	0.311	103.688
NSGAIII	50	50	50	842.741	3.370	0.357	68.073
MOPSO_FMF [19]	50	500	—	710.3	13.77	—	—
MOMA [21]	—	—	—	848.6486	5.1847	—	—
GROM [56]	50	100	—	851.23	7.01754	0.13789	—
TBLO [56]	50	100	—	854.0433	7.11366	0.13820	—
MOMVO [39]	50	500	—	797.2085	4.5205	—	—

Table 11: Validation of SC-2 Case 6 MOMA results against other algorithms.

Algorithm	Algorithm Parameters			Best compromise Solutions			Simulation Time (s)
	Population	Iterations	Pareto Solutions at Max. Iteration	Cost ($/h)	Loss (MW)	NLSI	
MOMA	20	50	20	850.053	3.925	0.153	42.958
MHHO	50	50	50	909.328	1.930	0.165	124.217
MOJAYA	50	50	27	859.636	3.357	0.159	79.673
MOPSO	50	50	50	859.695	2.336	0.291	96.097
NSGAIII	50	50	50	922.662	1.830	0.155	70.947

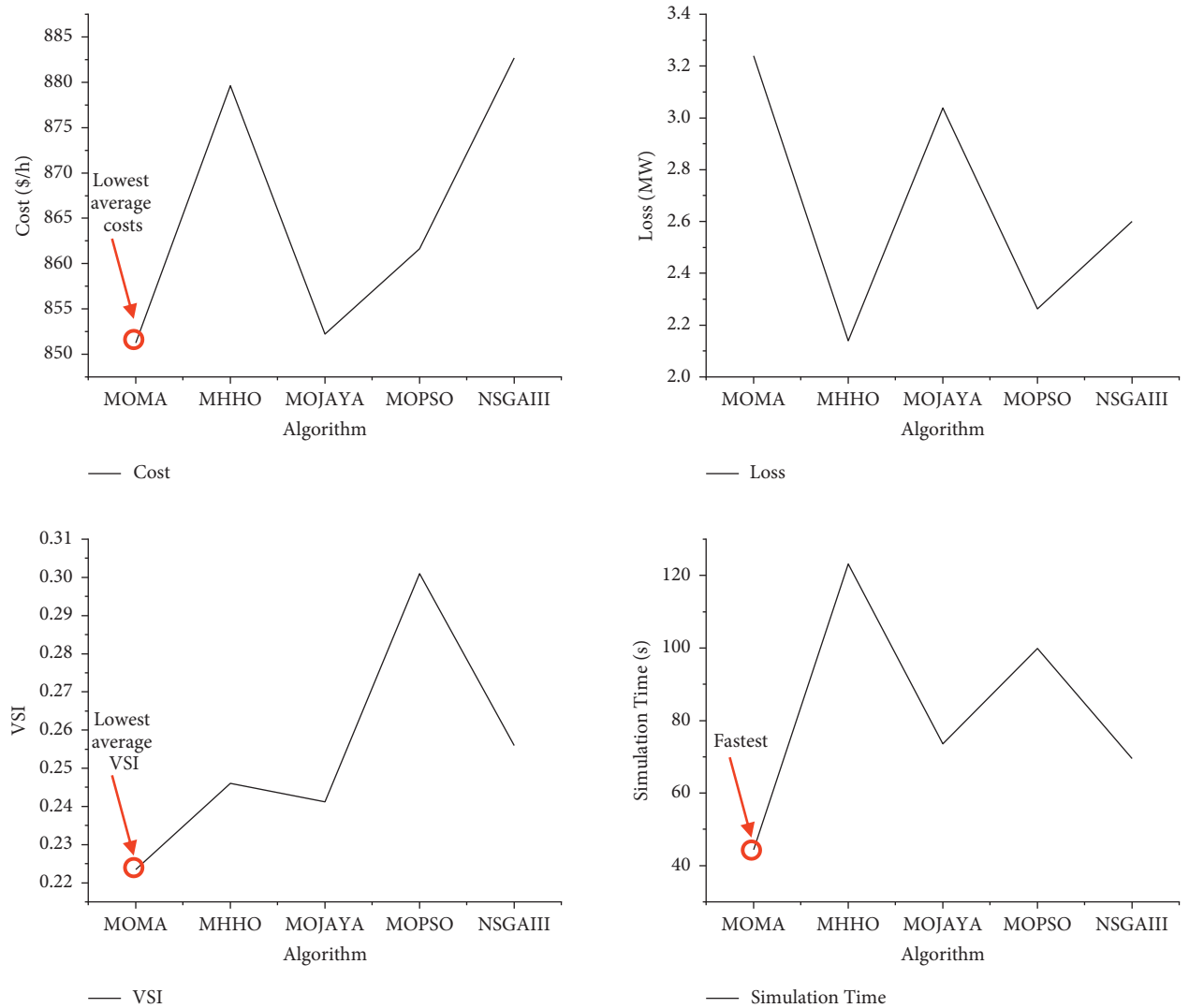

Figure 16: Dominance of MOMA algorithm in average system performance during SC-1 and SC-2.

Table 12: Validation of the proposed approach.

Approach	Description	Objective Function	Algorithm	VSI comparison	Best VSI	Cost ($/h)	Loss (MW)	Maximum VSI	RES?
Proposed method	Multi-objective based on Pareto optimality	Cost, Loss, VSI	MOMA	VCPI, LVSI, Lmn, FVSI, LQP, NLSI	VCPI	851.13	3.54	0.3641	Yes
Approach 1 [7]	Single objective	Cost	Improved Particle Swarm	L-index, FVSI, Lmn, LVSI, VCPI, FVSI	FVSI	845.189	6.12	—	No
Approach 1 [7]	Single objective	Loss	Improved Particle Swarm	L-index, FVSI, Lmn, LVSI, VCPI, FVSI	VCPI	978.00	3.269	—	No
Approach 1 [8]	Single objective	LVSI	DA-PSO	FVSI, Lmn, LVSI	LVSI	971.55	4.72	0.8072	No
Approach 1 [57]	Single objective	L-index	Symbiotic organisms search algorithm	—	L-index	926.923	4.5569	0.13671	Yes
Approach 2 [27]	Multi-objective based on weighted sum approach	—	Modified Interior Search	—	—	914.04	5.543	—	Yes

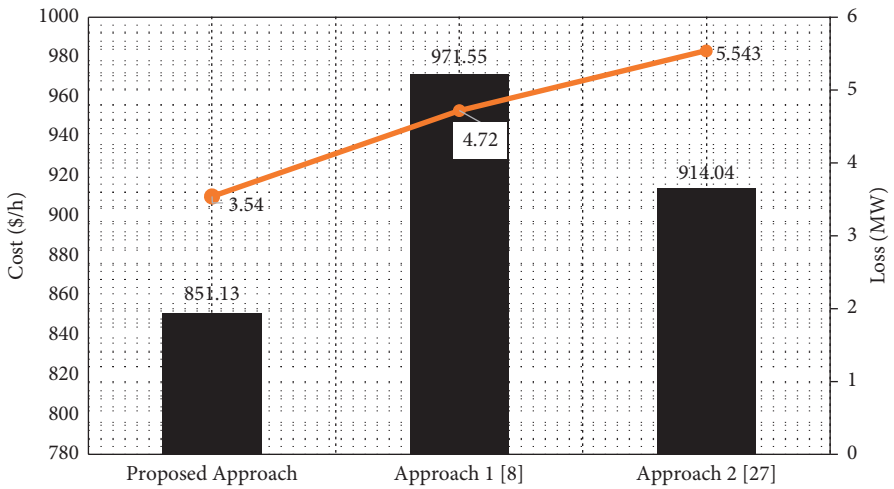

Figure 17: Comparison of the proposed approach against other methods.

renewables reduces negative environmental impact compared to conventional fossil fuel-based energy generation.

Figure 15 presents the average contribution of power from the different RES for all cases studies in both operating conditions.

The detailed results in Table 9 indicate that the NLSI, FVSI, and VCPI index led to the largest scheduled power of wind, solar PV, and hybrid wind/small hydro of 91.33%, 87.4%, and 84.5%, respectively. However, on a system average, the highest RES power-contributing VSI was the VCPI index, with the highest RES penetration level contribution of 16.61%.

6. Validation of Results

6.1. Validation of Algorithm. The results from the PSI ranking indicate the best voltage stability index to use in normal, and contingency conditions are VCPI and NLSI, respectively. Using these two indices, the results in normal conditions and contingency conditions were then validated against four other algorithms: multiobjective harris hawks algorithm (MHHO), multiobjective Jaya algorithm (MOJAYA), multiobjective particle swarm algorithm (MOPSO), and nondominated sorting genetic algorithm III (NSGA-III).

Results from the two operating scenarios (See Table 10 for SC-1 and Table 11 for SC-2) indicate that the multiobjective mayfly algorithm is the fastest, optimizing the system variables at an average speed of 106.72% faster than all other four algorithms. Additionally, the MOMA algorithm provided the greatest voltage stability improvement of 9.53%, 6.98%, 47.99%, 11.37% better than the MHHO, MOJAYA, MOPSO, and NSGAIII algorithms, respectively, in both normal and contingency operating conditions. On average, MOMA showed a dominant system performance during the two conditions (see

Figure 16). This is attributed to the algorithm's nuptial dance and random flight processes that enhance the balance between its exploration and exploitation properties and assist its escape from local optima [38].

6.2. Validation of Proposed Methodology. The proposed multiobjective approach provides the lowest system losses and generation costs by comparing the system's performance with previous research, as shown in Table 12 and Figure 17. Therefore, it demonstrates better system performance.

7. Conclusion

A comparison of the performance of six voltage stability indices in a multiobjective optimal power flow of a renewable energy integrated grid has been presented in this paper. The multiobjective mayfly algorithm minimized three objective functions: generation cost, active power loss, and voltage stability index. From the studies performed, the following deductions were made:

(i) The best VSI for improving system performance in normal operating conditions was the VCPI index, whereas it was the NLSI index in contingency conditions. However, an aggregated system performance in the two conditions indicated the VCPI is a superior index with an average PSI index of 0.9081, followed by the NSLI index of 0.8919.

(ii) The PSI best-performing indices are those with the least reactive power consumption in each operating scenario

(iii) The Lmn index ranked last in both operating conditions, resulting in the worst system performance in the highest generation cost, loss, and longest simulation time.

(iv) The VCPI index provided the largest average RES scheduled power of 82.54% to foster a high penetration of renewable energy sources on the system of 16.6%.

(v) There is a positive correlation between the increase in RES Scheduled Power and the average voltage stability enhancement of the system, as seen in the superior performance of the VCPI (highest average PSI rank) vs. its RES penetration levels.

(vi) The MOMA algorithm is superior to MOPSO, MOJAYA, NSGAIII, and MHHO algorithms in the studies carried out.

(vii) The proposed approach yields the lowest system costs and losses.

Incorporating voltage stability in the optimal power flow problem enhances the voltage stability of power systems with the integration of renewable energy sources. Specifically, the VCPI and NLSI indices show dominant performance in normal and contingency conditions.

The findings presented in this paper have substantial applicability in the planning of voltage stability enhancement for grids that incorporate renewable energy sources. Specifically, given the numerous voltage stability index computations, the approach in this work can serve as a practical guide for decision-makers when selecting indices that promote RES expansion and system stability improvement in modern energy management systems. Moreover, where cost and loss minimization are critical objectives, the voltage stability-constrained multiobjective optimal power flow assures that the aggregated system performance is improved across conflicting objectives.

With the increasing smart technologies, the proposed approach in this work is computationally efficient, achieving fast enhanced system performance in offline applications. However, techniques that incorporate stability prediction and training for real-time or online security monitoring would be significant. For future studies, a comparison of stability indices using such machine learning techniques for the real-time operation of power systems can be studied. Also, considering the numerous distributed energy resources in practical systems, it is unknown how the various voltage stability indices would perform in networks with increasing plug-in electric vehicles or battery energy storage systems. Therefore such studies can also be performed.

Data Availability

The research data used to support the findings of this study are included within the article.

Conflicts of Interest

The authors declare that they have no conflicts of interest.

References

[1] A. Abdollahi, A. Ghadimi, M. Miveh, F. Mohammadi, and F. Jurado, "Optimal power flow incorporating FACTS devices and stochastic wind power generation using krill herd algorithm," *Electronics*, vol. 9, no. 6, p. 1043, June. 2020.

[2] H. Zaheb, M. S. S. Danish, T. Senjyu et al., "A contemporary novel classification of voltage stability indices," *Applied Sciences*, vol. 10, no. 5, 2020.

[3] O. B. Adewuyi, H. O. R. Howlader, I. O. Olaniyi, D. A. Konneh, and T. Senjyu, "Comparative analysis of a new VSC-optimal power flow formulation for power system security planning," *Int. Trans. Electr. Energy Syst.*vol. 30, no. 3, Article ID e12250, March. 2020.

[4] M. H. Hassan, S. Kamel, A. Selim, T. Khurshaid, and J. L. Domínguez-García, "A modified rao-2 algorithm for optimal power flow incorporating renewable energy sources," *Mathematics*, vol. 9, no. 13, p. 1532, June. 2021.

[5] P. Sundaram and H. Jariwala, "Renewable energy resources integrated multiobjective optimal power flow using non-dominated sort Grey wolf optimizer," *J. Green Eng.*vol. 10, pp. 180–205, January. 2020.

[6] R. Kyomugisha, C. M. Muriithi, and M. Edimu, "Multi-objective optimal power flow for static voltage stability margin improvement," *Heliyon*, vol. 7, no. 12, Article ID e08631, December. 2021.

[7] S. Khunkitti, S. Premrudeepreechacharn, R. Chatthaworn et al., "A comparison of the effectiveness of voltage stability

indices in an optimal power flow," *IEEJ Transactions on Electrical and Electronic Engineering*, vol. 14, December. 2018.

[8] N. Thasnas and A. Siritaratiwat, "Implementation of static line voltage stability indices for improved static voltage stability margin," *J. Electr. Comput. Eng.*vol. 2019, Article ID 2609235, 14 pages, 2019.

[9] A. Estanqueiro and A. Couto, "New electricity markets. The challenges of variable renewable energy," in *Local Electricity Markets*, pp. 3–20, Elsevier, Amsterdam, Netherlands, 2021.

[10] N. Mlilo, J. Brown, and T. Ahfock, "Impact of intermittent renewable energy generation penetration on the power system networks - a review," *Technology and Economics of Smart Grids and Sustainable Energy*, vol. 6, no. 1, p. 25, December. 2021.

[11] J. A. Momoh, R. Adapa, and M. E. El-Hawary, "A review of selected optimal power flow literature to 1993. I. Nonlinear and quadratic programming approaches," *IEEE Transactions on Power Systems*, vol. 14, no. 1, pp. 96–104, 1999.

[12] M. A. Abido, "Optimal power flow using particle swarm optimization," *International Journal of Electrical Power & Energy Systems*, vol. 24, no. 7, pp. 563–571, 2002.

[13] D. Sun, B. Ashley, B. Brewer, A. Hughes, and W. Tinney, "Optimal power flow by Newton approach," *IEEE Transactions on Power Apparatus and Systems*, vol. PAS-103, no. 10, pp. 2864–2880, 1984.

[14] R. Mota-Palomino and V. H. Quintana, "A penalty function-linear programming method for solving power system constrained economic operation problems," *IEEE Power Engineering Review*, vol. PER-4, no. 6, p. 55, 1984.

[15] R. Burchett, H. Happ, and D. Vierath, "Quadratically convergent optimal power flow," *IEEE Transactions on Power Apparatus and Systems*, vol. PAS-103, no. 11, pp. 3267–3275, 1984.

[16] M. Rahli and P. Pirotte, "Optimal load flow using sequential unconstrained minimization technique (SUMT) method under power transmission losses minimization," *Electric Power Systems Research*, vol. 52, no. 1, pp. 61–64, 1999.

[17] P. P. Biswas, P. N. Suganthan, R. Mallipeddi, and G. A. J. Amaratunga, "Optimal power flow solutions using differential evolution algorithm integrated with effective constraint handling techniques," *Engineering Applications of Artificial Intelligence*, vol. 68, pp. 81–100, 2018.

[18] M. A. M. Shaheen, H. M. Hasanien, and A. Al-Durra, "Solving of optimal power flow problem including renewable energy resources using HEAP optimization algorithm," *IEEE Access*, vol. 9, pp. 35846–35863, 2021.

[19] M. A. Ilyas, G. Abbas, T. Alquthami, M. Awais, and M. B. Rasheed, "Multiobjective optimal power flow with integration of renewable energy sources using fuzzy membership function," *IEEE Access*, vol. 8, pp. 143185–143200, 2020.

[20] M. S. Syed, S. V. Chintalapudi, and S. Sirigiri, "Optimal power flow solution in the presence of renewable energy sources," *Iranian Journal of Science and Technology, Transactions of Electrical Engineering*, vol. 45, no. 1, pp. 61–79, March. 2021.

[21] A. K. Khamees, A. Y. Abdelaziz, M. R. Eskaros, H. H. Alhelou, and M. A. Attia, "Stochastic modeling for wind energy and multiobjective optimal power flow by novel meta-heuristic method," *IEEE Access*, vol. 9, pp. 158353–158366, 2021.

[22] S. Li, W. Gong, L. Wang, and Q. Gu, "Multiobjective optimal power flow with stochastic wind and solar power," *Applied Soft Computing*, vol. 114, Article ID 108045, January. 2022.

[23] A. Saha, A. Bhattacharya, P. Das, and A. K. Chakraborty, "A novel approach towards uncertainty modeling in multiobjective optimal power flow with renewable integration," *Int. Trans. Electr. Energy Syst.*vol. 29, no. 12, December. 2019.

[24] M. Farhat, S. Kamel, A. M. Atallah, and B. Khan, "Optimal power flow solution based on jellyfish search optimization considering uncertainty of renewable energy sources," *IEEE Access*, vol. 9, pp. 100911–100933, 2021.

[25] H. T. Kahraman and S. Duman, "Multiobjective adaptive guided differential evolution for multiobjective optimal power flow incorporating wind-solar-small hydro-tidal energy sources," in *Studies in Computational Intelligence*, pp. 341–365, Springer, Singapore, 2022.

[26] C. Srithapon, P. Fuangfoo, P. K. Ghosh, A. Siritaratiwat, and R. Chatthaworn, "Surrogate-assisted multiobjective probabilistic optimal power flow for distribution network with photovoltaic generation and electric vehicles," *IEEE Access*, vol. 9, pp. 34395–34414, 2021.

[27] N. Karthik, A. K. Parvathy, R. Arul, and K. Padmanathan, "Multiobjective optimal power flow using a new heuristic optimization algorithm with the incorporation of renewable energy sources," *International Journal of Energy and Environmental Engineering*, vol. 12, no. 4, pp. 641–678, December. 2021.

[28] Y. Li, Y. Li, G. Li, D. Zhao, and C. Chen, "Two-stage multiobjective OPF for AC/DC grids with VSC-HVDC: incorporating decisions analysis into optimization process," *Energy*, vol. 147, pp. 286–296, March. 2018.

[29] Y. Li and Y. Li, "Security-constrained multiobjective optimal power flow for a hybrid AC/VSC-mtdc system with lasso-based contingency filtering," *IEEE Access*, vol. 8, pp. 6801–6811, 2020.

[30] X. Liang, H. Chai, and J. Ravishankar, "Analytical methods of voltage stability in renewable dominated power systems: a review," *Electricity*, vol. 31 page, 2022.

[31] E. Kaymaz, S. Duman, and U. Guvenc, "Optimal power flow solution with stochastic wind power using the Lévy coyote optimization algorithm," *Neural Computing & Applications*, vol. 33, no. 12, pp. 6775–6804, June. 2021.

[32] S. B. Pandya and H. R. Jariwala, "A different perception of hybrid renewable energy sources integrated multiobjective optimal power flow considering performance parameters and penetration," *Smart Science*, vol. 9, no. 3, pp. 186–215, July. 2021.

[33] S. Gupta, N. Kumar, L. Srivastava, H. Malik, A. Anvari-Moghaddam, and F. P. García Márquez, "A robust optimization approach for optimal power flow solutions using Rao algorithms," *Energies*, vol. 14, no. 17, 2021.

[34] M. Rambabu, G. V. Nagesh Kumar, and S. Sivanagaraju, "Optimal power flow of integrated renewable energy system using a thyristor controlled SeriesCompensator and a grey-wolf algorithm," *Energies*, vol. 12, no. 11, p. 2215, June. 2019.

[35] S. Duman, S. Rivera, J. Li, and L. Wu, "Optimal power flow of power systems with controllable wind-photovoltaic energy systems via differential evolutionary particle swarm optimization," *Int. Trans. Electr. Energy Syst.*vol. 30, no. 4, April. 2020.

[36] H. Bouchekara, "Solution of the optimal power flow problem considering security constraints using an improved chaotic electromagnetic field optimization algorithm," *Neural Computing & Applications*, vol. 32, no. 7, pp. 2683–2703, 2020.

[37] M. Hemmati, B. Mohammadi-Ivatloo, and A. Soroudi, "Uncertainty management in decision-making in power system operation," in *Decision Making Applications in*

Modern Power Systems, pp. 41–62, Elsevier, Amsterdam, Netherlands, 2020.

[38] K. Zervoudakis and S. Tsafarakis, "A mayfly optimization algorithm," *Computers & Industrial Engineering*, vol. 145, Article ID 106559, July. 2020.

[39] M. Abdullah, N. Javaid, A. Chand, Z. A. Khan, M. Waqas, and Z. Abbas, "Multiobjective optimal power flow using improved multiobjective multi-verse algorithm," in *Advances in Intelligent Systems and Computing*, pp. 1071–1083, Springer, Berlin, 2019.

[40] S. Surender Reddy, P. R. Bijwe, and A. R. Abhyankar, "Real-time economic dispatch considering renewable power generation variability and uncertainty over scheduling period," *IEEE Systems Journal*, vol. 9, no. 4, pp. 1440–1451, December. 2015.

[41] M. Moghavvemi and O. Faruque, "Real-time contingency evaluation and ranking technique," *IEE Proceedings - Generation, Transmission and Distribution*, vol. 145, no. 5, p. 517, 1998.

[42] M. Moghavvemi and M. O. Faruque, "Technique for assessment of voltage stability in ill-conditioned radial distribution network," *IEEE Power Engineering Review*, vol. 21, no. 1, pp. 58–60, 2001.

[43] M. Moghavvemi and G. Jasmon, "New method for indicating voltage stability condition in power system," *IEE Int. Conf. Power Eng. Proc.*, pp. 223–227, January. 1997.

[44] I. Musirin and T. K. A. Rahman, "Novel fast voltage stability index (FVSI) for voltage stability analysis in power transmission system," in *Proceedings of the Student Conference on Research and Development*, pp. 265–268, Shah Alam, Malaysia, July 2002.

[45] A. Mohamed, G. B. Jasmon, and S. Yusoff, "A static voltage collapse indicator using line stability factors," *Journal of Industrial Technology*, vol. 17, no. N1, pp. 73–85, 1989.

[46] A. Yazdanpanah-Goharrizi and R. Asghari, "A novel line stability index (nlsi) for voltage stability assessment of power systems," in *Proceedings of the 7th WSEAS International Conference on Power Systems*, Beijing, China, September 2007.

[47] P. P. Biswas, P. Arora, R. Mallipeddi, P. N. Suganthan, and B. K. Panigrahi, "Optimal placement and sizing of FACTS devices for optimal power flow in a wind power integrated electrical network," *Neural Computing & Applications*, vol. 33, no. 12, pp. 6753–6774, Jun. 2021.

[48] P. P. Biswas, P. N. Suganthan, B. Y. Qu, and G. A. J. Amaratunga, "Multiobjective economic-environmental power dispatch with stochastic wind-solar-small hydro power," *Energy*, vol. 150, pp. 1039–1057, May 2018.

[49] P. P. Biswas, P. N. Suganthan, and G. A. J. Amaratunga, "Optimal power flow solutions incorporating stochastic wind and solar power," *Energy Conversion and Management*, vol. 148, pp. 1194–1207, 2017.

[50] N. Mujere, "Flood frequency analysis using the gumbel distribution," *International Journal on Computer Science and Engineering (IJCSE)*, vol. 3, 2011.

[51] Z. Liu, P. Jiang, J. Wang, and L. Zhang, "Ensemble forecasting system for short-term wind speed forecasting based on optimal sub-model selection and multiobjective version of mayfly optimization algorithm," *Expert Systems with Applications*, vol. 177, Article ID 114974, September. 2021.

[52] S. Hemamalini and S. P. Simon, "Economic/emission load dispatch using artificial bee colony algorithm," in *Proceedings of the Int. Conf. on Control, Communication and Power Engineering*, Chennai, India, July 2010.

[53] T. Niknam, M. R. Narimani, J. Aghaei, and R. Azizipanah-Abarghooee, "Improved particle swarm optimisation for multiobjective optimal power flow considering the cost, loss, emission and voltage stability index," *IET Generation, Transmission & Distribution*, vol. 6, no. 6, p. 515, 2012.

[54] K. Maniya and M. G. Bhatt, "A selection of material using a novel type decision-making method: preference selection index method," *Materials & Design*, vol. 31, no. 4, pp. 1785–1789, 2010.

[55] The University of Washington Electrical Engineering, "Power system test case archive, the IEEE 30-bus test system data," 1993, https://labs.ece.uw.edu/pstca/pf30/pg_tca30bus.htm.

[56] K. Nusair and F. Alasali, "Optimal power flow management system for a power network with stochastic renewable energy resources using golden ratio optimization method," *Energies*, vol. 13, no. 14, 2020.

[57] S. Duman, J. Li, and L. Wu, "AC optimal power flow with thermal-wind-solar-tidal systems using the symbiotic organisms search algorithm," *IET Renewable Power Generation*, vol. 15, no. 2, pp. 278–296, February. 2021.